We are IntechOpen, the world's leading publisher of Open Access books Built by scientists, for scientists

4,800
Open access books available

122,000
International authors and editors

135M
Downloads

Our authors are among the

154
Countries delivered to

TOP 1%
most cited scientists

12.2%
Contributors from top 500 universities

CLARIVATE ANALYTICS BOOK CITATION INDEX INDEXED

WEB OF SCIENCE™

Selection of our books indexed in the Book Citation Index in Web of Science™ Core Collection (BKCI)

Interested in publishing with us?
Contact book.department@intechopen.com

Numbers displayed above are based on latest data collected.
For more information visit www.intechopen.com

5

ZnO Nanorod Arrays Synthesised Using Ultrasonic-Assisted Sol-Gel and Immersion Methods for Ultraviolet Photoconductive Sensor Applications

Mohamad Hafiz Mamat[1], Zuraida Khusaimi[2], Musa Mohamed Zahidi[1] and Mohamad Rusop Mahmood[1,2]
[1]NANO-ElecTronic Centre (NET), Faculty of Electrical Engineering; [2]NANO-SciTech Centre (NST), Institute of Science (IOS); Universiti Teknologi MARA (UiTM), Shah Alam, Selangor, Malaysia

1. Introduction

Zinc oxide (ZnO) nanomaterials have emerged as one of the most promising materials for electronic devices such as solar cells, light-emitting devices, transistors, and sensors. The diverse structures of ZnO nanomaterials produce unique, useful, and novel characteristics that are applicable for high-performance devices. The ZnO nanorod array is a beneficial structure that has become extremely important in many applications due to its porosity, large surface area, high electron mobility, and variety of feasible techniques. The chemistry and physical tuning of its surface state, including processes such as annealing and chemical treatments, enhance its functionality and sensitivity and consequently improve the device performance. These useful characteristics of ZnO nanorod arrays enable the fabrication of ultraviolet (UV) photoconductive sensors with high responsivity and reliability. Although there are many techniques available to synthesise the ZnO nanorod arrays, solution-based methods offer many advantages, including the capacity for low-temperature processing, large-scale deposition, low cost, and excellent ZnO crystalline properties. In this chapter, the synthesis of ZnO nanorod arrays via ultrasonic-assisted sol-gel and immersion methods will be discussed for application to UV photoconductive sensors. The optical, structural, and electrical properties of deposited ZnO nanorod arrays will be reviewed, and the performance of the synthesised ZnO nanorod array-based UV photoconductive sensors will be discussed.

2. Ultraviolet photoconductive sensor using ZnO nanomaterials

Recently, ZnO nanostructures have received much attention due to their promising characteristics for electronic, optical, and photonic devices. Generally, ZnO exhibits semiconducting properties with a wide band gap of 3.3 eV at room temperature and a strong binding energy of 60 meV, which is much larger than that of gallium nitride (GaN, 25

meV) or the thermal energy at room temperature (26 meV). ZnO is naturally an n-type semiconductor material that is very transparent in the visible region, especially as a thin film, and has good UV absorption. ZnO is a biosafe and biocompatible material that has many applications, such as in electronics and biomedical and coating technologies. A reduction in size of the ZnO particle to the nanoscale level produces novel and attractive electrical, optical, mechanical, chemical, and physical properties due to quantum confinement effects. Moreover, ZnO nanostructures have a high aspect ratio, or a large surface-to-volume ratio and high porosity, which can fulfil the demand for high performance and efficiency in numerous applications (Lee et al., 2009, Galoppini et al., 2006, Park et al., 2011, Hullavarad et al., 2007).

UV photoconductivity, where the electrical conductivity changes due to the incident UV radiation, is characteristic of few semiconductors (wide band gap) or materials. This characteristic involves a number of mechanisms, including the absorption of light, carrier photogeneration, and carrier transport (Soci et al., 2010). Generally, a change in conductivity is related to the number of photogenerated carriers per absorbed photon or quantum yield and the mobility of the photogenerated carriers. The photoresponse time usually involves factors such as carrier lifetime and the defects state of the material. In other words, the UV photoconductivity represents important electrical properties that are related to carrier mobility, carrier lifetime, and defects in the materials.

There are various reports regarding UV photoconductive sensors that utilise ZnO nanostructures as the sensing elements. For example, Pimentel et al. developed ZnO thin-film-based UV sensors using radio frequency (RF) magnetron sputtering (Pimentel et al., 2006). They produced ZnO thin films with resistivities from 5 $x10^4$ to 1 $x10^9$ Ω cm and revealed that the preparation of ZnO films without oxygen exposure in an RF sputtering chamber produced a UV detector with higher sensitivity at thicknesses below 250 nm than ZnO films with oxygen exposure. They theorised that the result might have been due to the smaller grain size of the ZnO films without oxygen exposure, which increased the sensor active areas for UV detection.

Additionally, Xu et al. developed an Al-doped ZnO thin-film-based UV sensor using the sol-gel method (Xu et al., 2006). They produced a 5 mol % Al-doped ZnO film that was highly oriented along the c-axis of a Si (111) substrate. Their study detailed the suitability of Al-doped ZnO thin films for UV detection, where a high photocurrent value was obtained when the film was irradiated with UV light between 300 nm and 400 nm. However, their study revealed that the cut-off wavelength of Al-doped ZnO was blue-shifted to a shorter wavelength compared with the undoped film. They also observed that the photocurrent value of the Al-doped ZnO film in the visible region was reduced slightly compared to the undoped ZnO film, which improved the UV sensor sensitivity.

Zheng et al. developed a photoconductive ultraviolet detector based on ZnO films (Zheng et al., 2006). The ZnO thin films were deposited by pulsed laser deposition (PLD) at a thickness of 300 nm on glass substrates. Al metal contacts with 0.1 mm separation were deposited onto the ZnO films to complete the UV photoconductive sensor configuration. The crystallite size of the PLD-deposited ZnO film was around 23 nm, and the ZnO films grew along the c-axis, or perpendicular to the substrate. They found that the crystallite boundaries that were induced by the small crystallite size of the ZnO nanoparticles

contributed to the oxygen adsorption at the interfaces of the ZnO crystallites. This condition also resulted in carrier scattering, which decreased the carrier mobility. They also observed that the ZnO-nanoparticles based UV detector from their method showed a large dark current of approximately 0.2 mA at a bias voltage at 5 V, which was due to intrinsic defects, such as oxygen vacancies and zinc interstitials.

Jun et al. fabricated ultraviolet photodetectors based on ZnO nanoparticles with a diameter size of 70 nm using a paint method on thermally oxidised Si substrate (Jun et al., 2009). They used gold as the metal contacts with a gap of 20 μm. They addressed the surface defect problem experienced by nanoparticle-based UV detectors. Surface defects cause a rise time delay during UV illumination and irradiative recombination between the holes and electrons, which lowers the performance of ZnO nanoparticle-based devices.

Liu et al. fabricated a ZnO/diamond-film-based UV photodetector on a Si substrate (Liu et al., 2007). The ZnO films were deposited on a freestanding diamond-coated Si substrate by RF magnetron sputtering. They used gold as the metal contacts, which were deposited onto the film by DC magnetron sputtering with 2 mm of electrode separation. They found that the dark current of their UV sensor decreased with the grain size, which was due to the reduction of the ZnO grain boundaries. It was also mentioned that the ZnO-film-based UV photodetector showed a slow photoresponse due to a carrier-trapping or polarisation effect.

Hullavarad et al. developed UV sensors based on nanostructured ZnO spheres in a network of nanowires (Hullavarad et al., 2007). They produced the nanostructured ZnO using a direct vapour phase (DVP) technique. The sizes of the microspheres varied from 600 nm-2 μm, while the nanowire diameters were 30-65 nm. Based on their analysis, the dark current value of their sensor was 1×10^{-10} A at 1 V, which is less than the dark current of a ZnO thin film-based sensor reported by Yang et al. (Yang et al., 2003) and is a result of the low surface-defect properties of their ZnO nanostructures, as observed in the photoluminescence (PL) spectra.

Another interesting study that utilised a single nanobelt as a UV photoconductive sensor was conducted by Yuan et al. (Yuan et al., 2011). The nanobelt has a very similar structure as the nanorod, except the nanobelt exists in a box-like dimension where it has height (nanobelt thickness), width and length. In this case, the prepared nanobelt had a thickness of 120 nm and a width of 600 nm. With this structure, a sensor was constructed with a photocurrent value that was four orders of magnitude higher than the dark current. The sensor also possessed other excellent performance features, such as a high photosensitivity of 10^4, a low dark current of 10^{-3} μA, a low power consumption of 2.45 μW, a typical rise time of 0.12 s, and a decay time of 0.15 s. They explained that the high surface-to-volume ratio and the high coverage-area-to-total-area ratio contributed to the superior performance of their device.

A UV photoconductive sensor using a film of ZnO nanowall networks has been fabricated by Jiang et al. (Jiang et al., 2011). The films were prepared on a Si (111) substrate using plasma-assisted molecular beam epitaxy, with the inner diameters of the nanowalls ranging from 100 to 500 nm. In their sensor configuration, 200 nm-thick Au metal contacts were deposited in an interdigitated electrode design with electrode fingers that were 5 μm wide, 500 μm long, and on a pitch of 2 μm. The sensor showed a huge response to 352 nm UV light, with a responsivity of 24.65 A/W under a biased voltage of 5 V. The cut-off

wavelength of the sensor was approximately 360 nm. They showed that the nanostructure-based device had a high photoconductive gain due to the presence of oxygen-related hole-trap states on the nanowall surface.

Based on these previous studies, the use of nanostructure materials for UV photoconductive sensor applications have many advantages over bulk structures, including high gain, low power consumption, high sensitivity, reduced dimensionality, and the use of an extremely small fraction of the device's active materials. There are a number of factors that contribute to the high photosensitivity of nanostructure-based devices, including the surface-to-volume ratio, surface defects, light trapping, and porosity (Soci et al., 2007). Current research has mainly focused on the fabrication of UV photoconductive sensors using ultra-small nanostructures that contribute to the large surface area of the sensing element. Research has also emphasised prolonging the carrier lifetime of the device during UV illumination to lower the charge-carrier recombination. The carrier transit time also plays an important role in the device performance; thus, high mobility nanostructures are needed for good device performance.

3. ZnO nanorod arrays in ultraviolet photoconductive sensor

Currently, ZnO nanorods are receiving considerable attention for UV photoconductive sensor applications due to their unique characteristics and quantum confinement properties. The nanorod structure shows good surface area availability with excellence carrier transport characteristics that are very suitable for UV sensor applications. Depending on the method and experimental parameters used, the nanorod sizes (i.e., diameter and length) are tuneable, which may give different sensor performances. Additionally, by modifying the surface, the performance of the sensor can also be improved because of the relationship between surface defects and surface adsorption of gas molecules from the atmosphere, which tremendously influence the sensor characteristics. According to Soci et al., one-dimensional (1D) structures have several advantages over bulk or thin films in UV sensor applications, including light scattering enhancements that reduce optical losses, improved light absorption, large photosensitivity due to the high gain, and the possibility to integrate functionalities within single 1D devices (Soci et al., 2010). The prolonged photocarrier lifetime, which is due to charge separation promoted by surface states, and the reduction in carrier transit time, which can be achieved in high-quality, low-defect ZnO nanorod together with small gap of metal contacts, both contribute to the high gain in the nanorod-based devices.

Surface area plays a very important role in the UV sensing mechanism, as the sensing mechanism involves the surface reactions between free carriers and the surrounding environment, such as oxygen molecules and humidity (Mamat et al., 2011). The nanorod area possesses a high surface area on the film surface that is suitable for UV photoconductive sensor applications. Moreover, these nanorods exhibit higher carrier mobility than that of ZnO nanoparticles, which works effectively during the surface reaction process. Generally, the photoresponse of a UV photoconductive sensor is influenced by the adsorption and desorption of oxygen on its surface during UV illumination. Oxygen molecules from the surrounding are adsorbed onto the nanorod surface by capturing free electrons from ZnO, as shown in the following equation (Su et al., 2009, Zheng et al., Lupan et al., 2010):

$$O_2 + e^- \rightarrow O_2^- \tag{1}$$

where O_2 is an oxygen molecule, e^- is a free electron, and O_2^- is an adsorbed oxygen on the nanorod surface. When the UV light is incident on the nanostructure surface, electron-hole pairs are photogenerated according to the following equation:

$$hv \rightarrow h^+ + e^- \tag{2}$$

where hv is the photon energy of UV light, h^+ is a photogenerated hole in the valence band and e^- is a photogenerated electron in the conduction band. A large surface area availability in the nanorod film facilitates a fast surface reaction process as the photogenerated hole reacts with a negatively charged adsorbed oxygen, as shown by:

$$O_2^- + h^+ \rightarrow O_2 \tag{3}$$

This condition leaves behind the electron of the pair, which increases the conductivity of the nanostructures. When the illumination is turned off, the oxygen molecule recombines with the electron, leading to a decrease in film conductivity.

This sensor behaviour that is related to the adsorption and desorption of oxygen was studied by Jun et al. (Jun et al., 2009). They measured their fabricated UV sensor under different atmospheric pressures (0.1-1 atm), with different oxygen levels. They found that the photoresponse decay time constant of the sensor increased with decreasing atmospheric pressure. Because the lower atmospheric pressure had a lower oxygen content, it reduced the ability of the sensor to return to its initial state (dark current) due to a reduction of oxygen adsorption onto the ZnO surface. This condition increased the decay time constant of the device as the atmospheric pressure was lowered.

Basically, the nanorod-based UV photoconductive sensor represents the simplest configuration of the UV sensor. It consists of just the nanorods and metal contacts for the photogenerated carrier transport to the outer circuit. In this UV photoconductive sensor configuration, ZnO nanorods are used either vertically or horizontally with the substrates. The vertical standing nanorod is commonly used in an array form or a film-based sensor, while the horizontal nanorod is used in single-nanorod-based sensors. However, a single-nanorod-based UV sensor is very complicated and involves a very challenging fabrication process using high-cost instruments. The realisation of single-nanorod-based UV sensors might reduce the size and the power consumption of the UV sensor. For example, a single-ZnO-nanorod-based UV sensor has been fabricated by Chai et al. (Chai et al., 2011). They used chemical vapour deposition (CVD) method to synthesise a ZnO nanorod with a diameter approximately 1-3 μm and a length of 20-200 μm. To fabricate the UV sensor, a focused ion beam (FIB) *in situ* lift-out technique was used. In their sensor configuration, Au/Ti metal electrodes separated by 20 μm were used. They showed that the single nanowire had a good response to UV light, where the resistance decreased from 52.4 to 48.0 kΩ during 365 nm UV illumination with an optical power of 0.1 mW.

A nanorod array-based UV photoconductive sensor is a promising device structure that has an easier fabrication process compared to a single nanorod-based UV sensor. Moreover, it produces large photocurrent signals due to the large surface coverage and nanorod density.

Various techniques are available to fabricate the ZnO nanorod array, including metal-organic chemical vapour deposition (MOCVD), CVD, sputtering, and solution-based synthesis. Solution-based synthesis has shown promising results for producing aligned ZnO nanorod arrays. This technique is simple, versatile, low-temperature and can be used for large-scale depositions. Another advantage of this technique is that it is a vacuum and gas-free deposition method in which the chemical reactions completely depend on the prepared solution. The biggest advantage of this method is its low-temperature processing, which could even be used to deposit nanostructures on polymer substrates. Unlike other methods that require high temperature for nanostructure growth, this hydrothermal synthesis can be operated at temperatures as low as 50°C for the deposition of ZnO nanostructures (Niarchos et al., 2010).

4. Synthesis of ZnO nanorod arrays via ultrasonic-assisted sol-gel and immersion methods

Recently, ultrasonic irradiation has been applied in hydrothermal processes to prepare ZnO nanostructures. This sonochemical methods use ultrasound irradiation at ranges between 20 kHz to 10 MHz (Suslick et al., 1991). For example, Mishra et al. have synthesised flower-like ZnO nanostructures using a starch-assisted sonochemical method (Mishra et al., 2010). Jia et al. also produced ZnO nanostructures using a sonochemical method (Jia et al., 2010). Using ultrasonic irradiation, they produced hollow ZnO microspheres during hydrothermal synthesis. Another example of ultrasonic-assisted hydrothermal synthesis is a study performed by Mazloumi et al. They produced cauliflower-like ZnO nanostructures using a sonochemical method (Mazloumi et al., 2009). The products that were synthesised by the three sonication methods were similar in that they consisted of powder-form nanostructures. Unfortunately, the powder-forms structures require a seperate process to deposit them onto the substrate for electronic device applications.

In our process, we apply ultrasonic irradiation to the precursor solution, which is used to grow ZnO nanorod arrays on a seed-layer-coated substrate using an immersion process. The sonication process uses powerful ultrasound radiation that can induce molecules to undergo chemical reactions. Sonication is usually used in cleaning processes to remove contaminations, such as substrate and glass wear, from solid surface. Ultrasound radiation involves the creation, growth and collapse of bubbles that can break the chemical bonds of materials in a liquid medium. Generally, growing nanomaterials using a chemical solution method requires a precursor, stabiliser, and solvent. The precursor material supplies the main atoms or ions of the nanomaterials, while the stabiliser material is used to ensure that the growth of the nanomaterial is controlled to a specific rate or structure. The reaction process between the stabiliser and the precursor material prevents the nanomaterials from growing too fast in a certain direction or plane. However, if the reaction process between the precursor and stabiliser does not occur uniformly throughout the solution (e.g., due to agglomerated precursor materials at the beginning or early stages), the size of the end product materials will be large, consequently reducing the surface area. This condition reduces the quantum confinement effect in the produced nanomaterials. In our case, we apply sonication to rupture agglomerated precursor and stabiliser materials and, at the same time, ensure a highly homogenous and uniform reaction process between the precursor and stabiliser.

ZnO nanorod array films were fabricated using an ultrasonic-assisted sol-gel and immersion method using zinc nitrate hexahydrate ($Zn(NO_3)_2 \cdot 6H_2O$) as a precursor, hexamethylenetetramine (HMT, $C_6H_{12}N_4$) as a stabiliser, and aluminium nitrate nonahydrate ($Al(NO_3)_3 \cdot 9H_2O$, 98 %, Analar) as a dopant (Mamat et al., 2010). Aluminium (Al) doping is especially attractive because it contributes to the higher conductivity of the film without deteriorating the optical and crystalline properties of the ZnO. The precursor, stabiliser, and dopant were dissolved in deionised (DI) water before being subjected to the sonication process using an ultrasonic water bath (Hwasin Technology Powersonic 405, 40 kHz) for 30 min at 50°C. Subsequently, the solution was stirred and stored at room temperature for 3 h.

Next, the solution was poured into a vessel, where the seed-layer–coated glass substrate was positioned at the bottom of the vessel. The seed layer, or Al-doped ZnO nanoparticle layer, was coated onto the substrate with a thickness of approximately 200 nm using sol-gel spin-coating (Mamat et al., 2010). The existence of the seed layer on the glass substrate reduced the formation energy for the crystallisation of the ZnO and, thus, helped the nanorod grow more easily on the glass substrate. The vessel was then sealed before being immersed into a water bath for 4 h at 95°C. After the immersion process, the sample was removed from the vessel and rinsed with DI water. The sample was then dried at 150°C for 10 min and annealed at 500°C for 1 h in a furnace. Next, 60-nm-thick Al metal contacts were deposited onto the nanorod array using thermal evaporation to complete the sensor structure. The distance between the electrodes was approximately 2 mm.

The surface morphologies of the ZnO nanorod array films were observed by field-emission scanning electron microscopy (FESEM, ZEISS Supra 40VP and JEOL JSM-7600F). The surface topology of the nanorod arrays was characterised using atomic force microscopy (AFM, Park System). The crystallinity of the samples was investigated using X-ray diffraction (XRD, Rigaku Ultima IV). The transmittance and absorbance characteristics of the seed layer and the thin film were characterised using an ultraviolet-visible (UV-Vis) spectrophotometer (Perkin Elmer Lambda 750). The photoluminescence (PL) properties of the synthesised nanorods were investigated using a PL spectrophotometer with a helium-cadmium (He-Cd) excitation laser operating at 325 nm (PL, Horiba Jobin Yvon-79 DU420A-OE-325). The UV photoresponse measurements of the fabricated sensor were conducted using a spectral sensitivity analysis system (Bunko-Keiki, CEP 2000) with a monochromatic xenon (Xe) lamp operating at 365 nm and a power intensity of 5 mW/cm^2 as well as photocurrent measurement system operating at 365 nm and a power density of 750 $\mu W/cm^2$. The thicknesses of the samples were measured using a surface profiler (VEECO/D 150+). The fabrication process of the ZnO-nanorod-based UV photoconductive sensor is shown in Fig. 1.

5. Performance of synthesised ZnO-nanorod-array-based ultraviolet photoconductive sensor

We have investigated the performance of the ZnO-nanorod-array-based UV photoconductive sensor prepared via ultrasonic-assisted sol-gel and immersion methods. There are numerous factors that influence the sensor performance, such as nanorod size, surface area, surface defects, film thickness, metal contacts, and doping. In this subchapter, we will highlight the effects of surface modifications, film thickness, and Al ions doping on the performances of the fabricated ZnO-nanorod-array-based UV sensor.

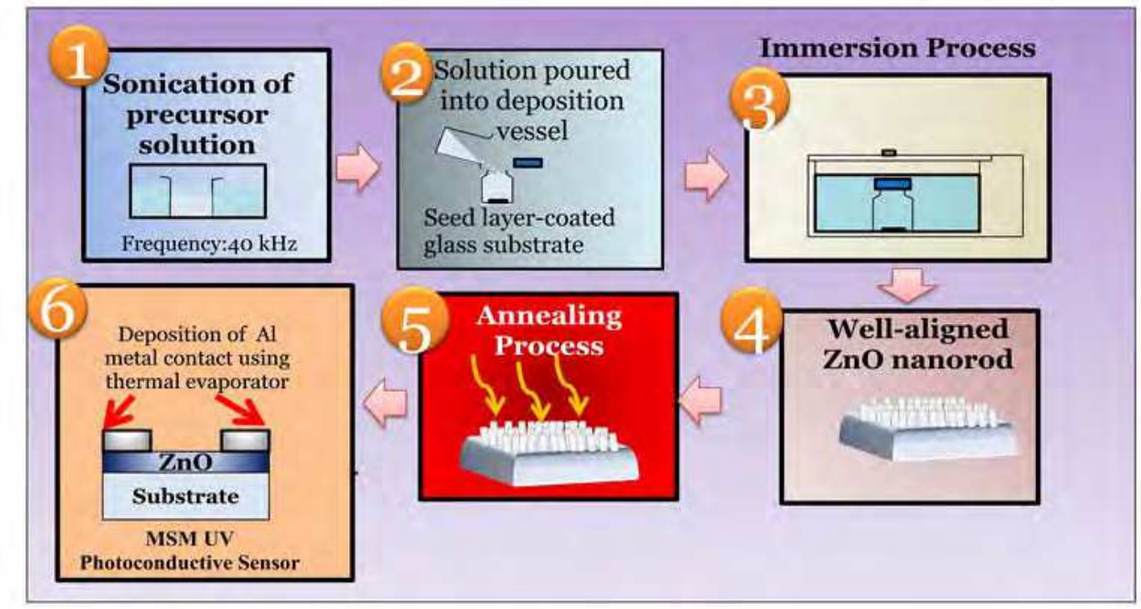

Fig. 1. Fabrication process of aligned ZnO nanorod array-based UV photoconductive sensor via sonicated sol-gel and immersion methods.

5.1 Surface modification

A ZnO nanorod array was prepared on glass substrate utilising an Al-doped ZnO nanoparticle thin film catalytic seed layer. Figure 2(a) shows a field-emission scanning electron microscopy (FESEM) image of the seed layer that was prepared using the sol-gel spin-coating technique. The particle sizes of the Al-doped ZnO nanoparticles were estimated to range from 10 to 40 nm. From the FESEM figure, synthesised Al-doped ZnO nanoparticles exhibited some edges rather than perfect curved surfaces due to the differenced in the surface energy of crystallographic directions of the ZnO growth. In the wurtzite structure, the relative growth rate of each crystallographic plane differed somewhat according to the crystal orientation, so it was difficult for crystalline ZnO to grow symmetrically into spherical particles (Lee et al., 2007). The FESEM figure also indicates that the particles were well connected to each other and that it was very important to develop a continuous transport pathway in the granular film for electron movement in the UV sensor application. Figure 2(b) shows an AFM image of the seed catalyst layer. Based on the AFM image, the root mean square (RMS) roughness of the Al-doped ZnO nanoparticle thin film was 17.51 nm over an area of 100 μm^2.

In the UV photoconductive sensor, this seed layer plays a very important role in increasing the sensor performance. Generally, one of the factors that degrades the sensor performance is the strain of the film or the material, which influences the density of the defects and the photoelectric activity of the sensor (Shinde & Rajpure, 2011). This seed layer facilitates the homogenous growth of the compressive-strained layer, i.e., the high quality ZnO nanorod material, which has a low defect density and allows for a smooth charge transfer process during UV photo-illumination. As a result, the seed layer results in a higher responsivity of the ZnO-nanorod-array-based UV photoconductive sensor.

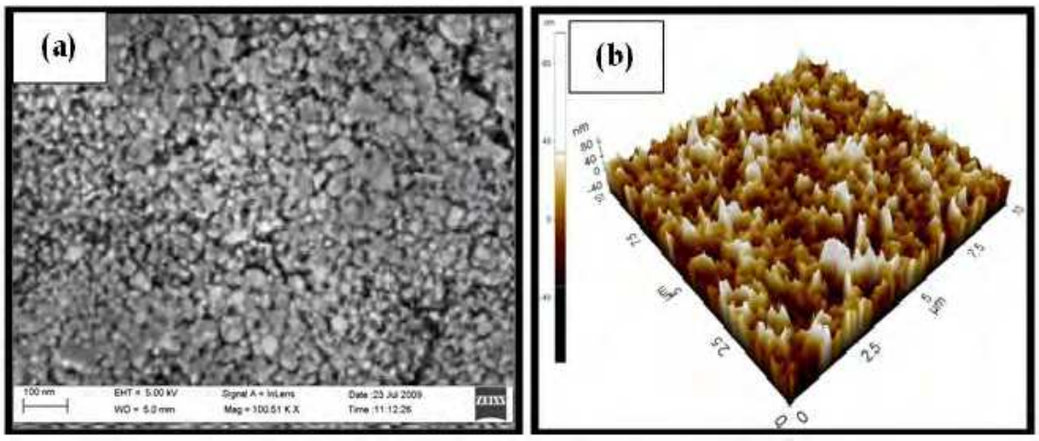

Fig. 2. (a) FESEM image of Al-doped ZnO nanoparticle thin film seed layer. (b) AFM topography image of the seed layer.

Figure 3 shows an FESEM image of the Al-doped ZnO nanorod array before (Fig. 3(a)) and after (Fig. 3(b) and 3(c)) the annealing process at 500°C. The nanorods were prepared using a 1000 ml solution that was sonicated in a beaker. The images show that well-oriented, hexagonal-shaped ZnO nanorod arrays were deposited onto the seed-layer-coated glass substrate with good uniformity and high density. The diameters and lengths of the nanorods were not strongly affected by the annealing process, as the diameter of the nanorods ranged between 40 to 150 nm and the nanorods were 1.1 µm long. The nanorods were aligned well, which indicates that this low-temperature ultrasonic-assisted sol-gel and immersion processes produce high-quality ZnO nanorod arrays. We believe that the excellent alignment of the nanorod arrays is due to the seed layer films, which act as nucleation centres that provide an almost mismatch-free interfacial layer between the nanorods and the seed layers. This layer assists an epitaxial nanorod growth process on the seed-layer-coated glass substrates. Figure 3(d) shows an AFM topography image of an annealed ZnO nanorod array measured in a 1 μm^2 area. Based on this topography image, the root mean square (RMS) roughness of the nanorod array was approximately 21.95 nm.

As shown in Fig. 3(b) and 3(c), nanoholes appeared on the surfaces of the nanorods after the annealing process. A closer look at the cross-sectional images indicates that nanoholes exist on nearly the entire nanorod surface. We suspect that these nanoholes are the result of the evaporation of impurities, such as hexamethylenetetramine (HMT), during the annealing process at high temperature. Interestingly, these nanoholes facilitate a larger surface area availability of the single nanorod and facilitate effective sites for the oxygen adsorption process. Thus, the existence of these nanoholes on the nanorod surface could improve the performance of the UV photoconductive sensor because of the increased surface area and surface photochemistry. The condition of the Al-doped ZnO nanorod with nanoholes after annealing process is shown in Fig. 4.

XRD spectra of the as-grown nanorods and the 500°C annealed nanorods are shown in Figure 5. The spectra confirmed that the synthesised nanorods belong to the ZnO hexagonal wurtzite structure (joint committee on powder diffraction standards (JCPDS) PDF no. 36-1451). Both the as-grown and annealed samples contained a dominant XRD peak at the

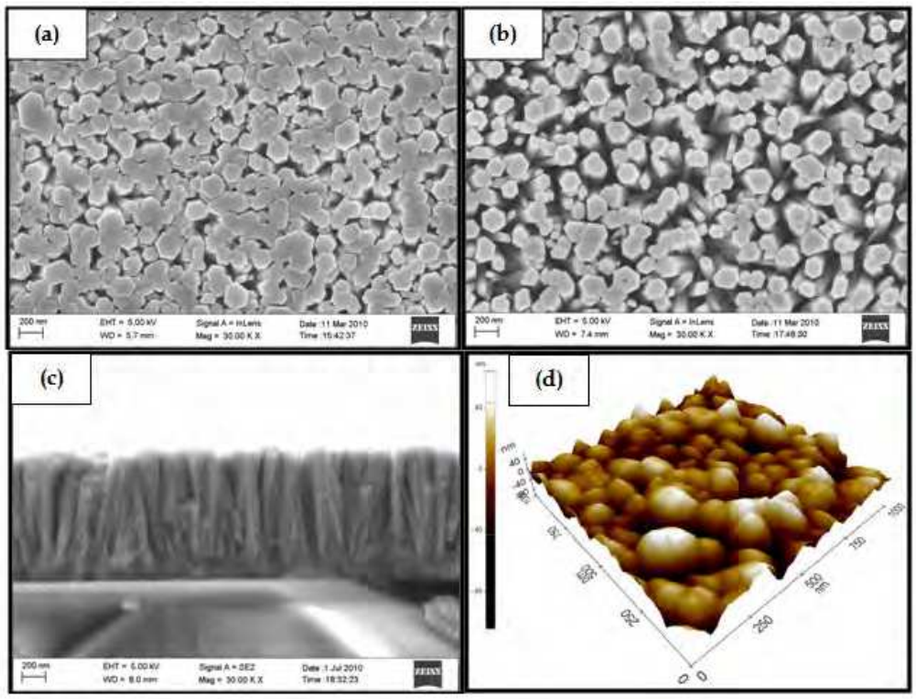

Fig. 3. FESEM image of (a) as-grown and (b) 500°C annealed Al-doped ZnO nanorod arrays. (c) Cross-sectional image of the annealed Al-doped ZnO nanorod arrays, clearly showing nanoholes on the ZnO surface. (d) AFM image of the annealed Al-doped ZnO nanorod array.

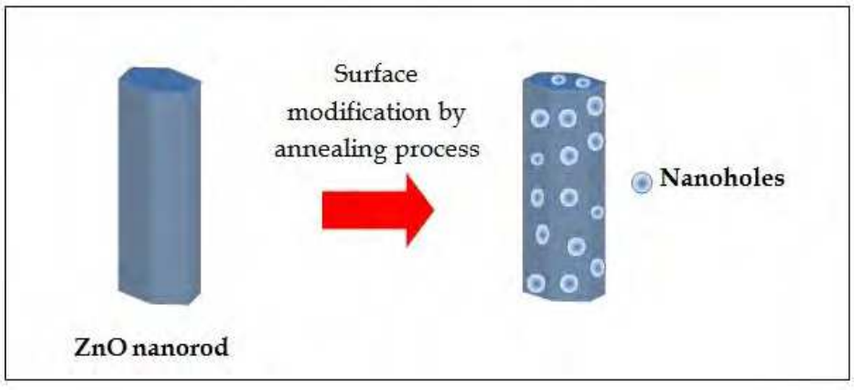

Fig. 4. Nanoholes produced on the surface of the nanorod after the annealing process as a result of the evaporation of impurities.

(002)-plane, implying that the nanorods were grown along the c-axis, or perpendicular to the substrates. This result indicates that the Al-doped ZnO nanorod arrays prepared in this work had a very good ZnO crystal quality. The weak peaks intensities of the other orientations might be due to the vertical alignment imperfections of the nanorods (Qiu et al., 2009). Based on the spectra, the peak intensities of the annealed nanorods were higher than the as-grown sample, indicating an improvement in the nanorod crystallinity after the annealing treatment. Based on these results, we predicted a possible growth mechanism for

the formation of the well-aligned ZnO nanorod arrays on the seed-layer-coated glass substrate using the ultrasonic-assisted sol-gel and immersion methods (Mamat et al., 2011). We suspect that the growth along the c-axis might be caused by the effects of the sonication process on the precursor solution, which disperses and mixes the zinc nitrate (i.e., the precursor), aluminium nitrate (i.e., the dopant), and the HMT (i.e., the stabiliser) very well. The sonication process also helps dissolve the agglomerated zinc nitrate and HMT particles, which hasten the physical and chemical reaction activity in the solution. This process enables the Zn^{2+} ion to react effectively with the HMT, as shown by (Khusaimi et al., 2010)

$$Zn(NO_3)_2 + C_6H_{12}N_4 \rightarrow [Zn(C_6H_{12}N_4)]^{2+} + 2NO_3^- \quad (4)$$

The HMT plays a very important role in controlling the growth of the aligned ZnO nanorods. When it attaches to the Zn^{2+} ions, particle agglomeration is reduced and ZnO formation in the solution is slowed.

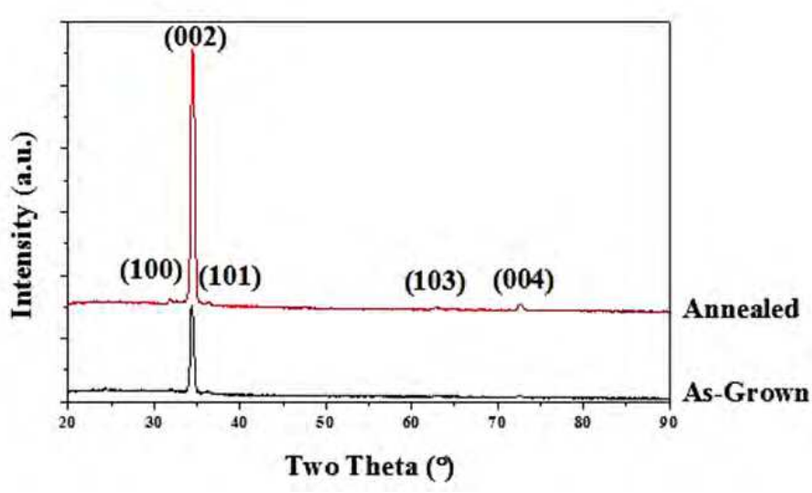

Fig. 5. XRD patterns of Al-doped ZnO nanorod array before (as-grown) and after annealing.

During the hydrothermal process, the seed catalyst layer provides a base that initiates the growth of the nanorod arrays through heterogeneous nucleation. It is generally accepted that heterogeneous nucleation on a seed layer surface occurs more easily than does homogenous nucleation (Guo et al., 2005). The seed layer provides the lowest energy barrier for heterogeneous nucleation, which produces almost negligible lattice mismatch between the nanorods (Chen et al., 2009, Giri et al., 2010). This condition results in the growth of high-quality aligned nanorod arrays on the substrates. The general reactions occurring during the hydrothermal process can be described by the following equations (Khusaimi et al., 2010, Lupan et al., 2007):

$$C_6H_{12}N_4 + 4H_2O \rightleftharpoons C_6H_{12}N_4H_4^+ + 4OH^- \quad (5)$$

$$[Zn(C_6H_{12}N_4)]^{2+} + 4OH^- \rightarrow Zn(OH)_4^{2-} + C_6H_{12}N_4 \quad (6)$$

$$Zn(OH)_4^{2-} \rightarrow Zn^{2+} + 4OH^- \quad (7)$$

$$Zn^{2+} + 2OH^- \rightleftharpoons ZnO + H_2O \text{ or } Zn^{2+} + 2OH^- \rightleftharpoons Zn(OH)_2 \rightleftharpoons ZnO + H_2O \quad (8)$$

Initially, when the Zn^{2+} and OH^- ion concentrations exceed the boundaries of supersaturation, ZnO nuclei form on the seed layer surface, initiating the growth of aligned ZnO nanorods. It has been suggested that the HMT also acts as a chelating agent that attaches to the nonpolar facets of ZnO nanorods (Sugunan et al., 2006). Because of this attachment behaviour, epitaxial growth along the c-axis is facilitated because only the (0001) plane is exposed during the growth process. Because the growth rate in the (0001) plane proceeds the fastest in the hydrothermal system (Laudise & Ballman, 1960, Laudise et al., 1965), the ZnO nanorods grow preferentially in the (0001) plane, which is vertically aligned with the substrate.

Good dispersion and mixing processes between the precursor and the stabiliser through sonication help control the diameter sizes of the nanorods because the HMT can immediately attach onto the nonpolar facets (i.e., six prismatic side-planes) after the ZnO nanorod nucleation process is initiated on the seed layer. The HMT acts as a buffer layer at the nonpolar surfaces, which disturbs the ZnO deposition onto these surfaces. This condition disables rapid growth on the side walls, or the nonpolar surface of the nanorod, which served to maintain an almost constant diameter size throughout the length. The rapid attachment of the HMT onto the ZnO surface prevents any nanorod growth in the direction of the nonpolar facets, thus hindering an enlargement in the nanorod diameter. Therefore, because the ZnO nanorods are confined by the HMT molecules on their nonpolar surfaces and only grow from the polar surface for further growth, directional growth along the c-axis is achieved.

The photoluminescence (PL) spectra of the as-grown nanorod and the annealed nanorod with nanoholes are depicted in Fig. 6. The main peaks that were observed in the spectrum of the annealed nanorods are located at 380 and 580 nm, and the main peaks in the spectrum of the as-grown nanorods is located at 380 and 590 nm. The UV emission at 380 nm corresponds to free exciton recombination, while the orange emission at 580 and 590 nm are related to the emission from defects, such as oxygen deficiencies and zinc interstitials. According to Rosa et al., this orange emission is due to zinc interstitials that occur close to or on the surface of the ZnO structure (De la Rosa et al., 2007). The shift in the visible emission peak from 590 to 580 nm for annealed nanorods might be due to the desorption of the OH groups from the nanorod surface (Lee et al., 2010). The as-grown nanorods exhibited a very weak UV emission peak intensity compared to the annealed nanorods. The annealing process increased the UV emission peak intensity, which indicates that the crystallinity of the sample improved at the higher annealing temperatures.

During the annealing treatment, the concentrations of defects in the nanorods were reduced according to equations (9-10) shown below (Lin et al., 2001):

$$V_O + \frac{1}{2}O_2 = O_O \tag{9}$$

$$Zn_i + \frac{1}{2}O_2 = Zn_{Zn} + O_O \tag{10}$$

where V_O is an oxygen vacancy, Zn_i is a zinc interstitial, and Zn_{Zn} and O_O represent zinc and oxygen at a lattice site, respectively. Because the supplied thermal energy induces an oxygenation process during the annealing treatment, oxygen from the atmosphere occupies the vacant sites of the ZnO lattice, which eventually reduces both the zinc interstitial and

oxygen vacancy concentrations. To investigate this phenomenon, we calculated the ratio of the UV emission intensity over the visible emission intensity to be 0.6 and 7.1 for the as-grown and the 500°C annealed nanorods, respectively. It is generally accepted that this ratio value is a good way to evaluate the optical quality and stoichiometric properties of ZnO. An increase of this ratio indicates that the stoichiometric properties of ZnO and its optical properties were improved after the annealing process. Lee et al. reported that the ratio of the UV peak intensity over the visible peak intensity is directly related to the oxygen deficiency in the ZnO nanorods (Lee et al., 2010). Based on this ratio analysis, the defect concentrations from oxygen vacancies and zinc interstitials were suppressed during the annealing treatment, as indicated by in equations (9-10). The reduction of defect concentrations in the nanorods strengthened the UV emission and reduced the visible emission of the nanorods after the annealing process.

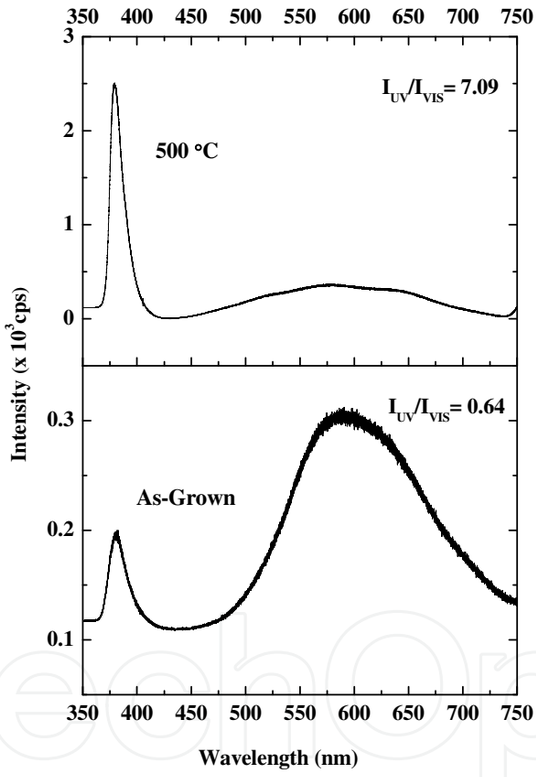

Fig. 6. Room temperature PL spectra of the as-grown and annealed ZnO nanorod arrays.

Figure 7 shows the time-dependent photocurrent properties of the fabricated UV photoconductive sensors under a bias voltage of 10 V. The measurements were conducted using 365 nm UV illumination with an optical power density of 5 mW/cm2. Both the as-grown and annealed nanorods showed a response to the UV light but with different sensing characteristics. The dark currents/photocurrents of the fabricated devices were 3.49 x 10^{-6} A/4.08 x 10^{-4} A and 1.78 x 10^{-6} A/1.35 x 10^{-4} A for the annealed and as-grown nanorods, respectively. The responsivity of the fabricated devices was calculated according to equation (11) (Jun et al., 2009):

$$R = \frac{I_{ph} - I_{dark}}{P_{op}} \tag{11}$$

where I_{ph} is the photocurrent, I_{dark} is the dark current, and P_{op} is the optical power of the UV source. For the annealed nanorod-array-based UV sensor, the calculated responsivity was 1.35 A/W. For the as-grown nanorod-array-based UV sensor, the responsivity was 0.44 A/W. The desirable crystallinity properties and low defect concentrations of the annealed nanorods may have contributed to the high responsivity of this sensor. The rise and decay time constants for the fabricated sensors were estimated using equations (12-13) (Jun et al., 2009, Li et al., 2009):

Rise process upon UV illumination ON:

$$I = I_0\left(1 - e^{\frac{-t}{\tau_r}}\right) \tag{12}$$

Decay process after UV illumination OFF:

$$I = I_0 e^{\frac{-t}{\tau_d}} \tag{13}$$

where I is the magnitude of the current, I_0 is the saturated photocurrent, t is time, τ_r is the rise time constant and τ_d is the decay time constant. The calculations show that the annealed Al-doped ZnO nanorod array-based UV sensor exhibited small rise and decay time constants at 20 s and 22 s, respectively. For the as-grown sample, the rise time constant was 280 s, while the decay time constant was estimated to be 300 s. This result indicates that the annealing process greatly improved the performance of the UV sensor.

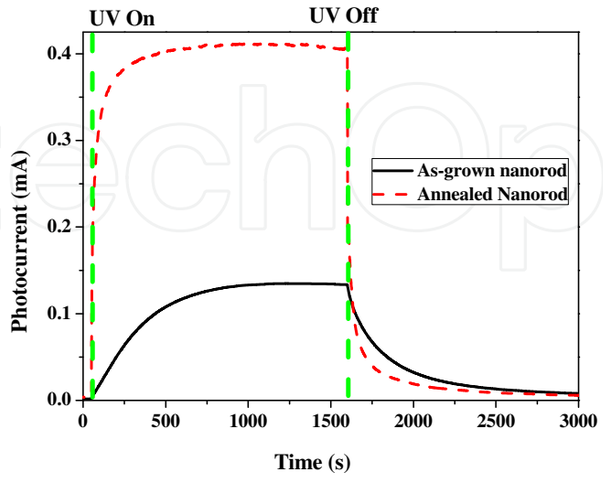

Fig. 7. Plot of the growth and decay of the photocurrent measured at 10 V of the as-grown and annealed Al-doped ZnO nanorod array-based UV photoconductive sensors under 365 nm, 5 mW/cm² UV illumination.

The annealing process plays an important role in improving the sensor performance and is considered a surface treatment or surface modification. For example, Kim et al. reported that water molecules and residual carbon from the fabrication process could be effectively desorbed from the surface of a ZnO nanowire during the annealing process (Kim et al., 2011). As a consequence, oxygen molecules from the air could occupy the existing defect sites more easily, which contributed to a faster photocurrent decay, higher sensitivity, and faster response when the UV light was turned off. Because their fabricated sensor consisted of a ZnO nanowire network that depended on the interconnections between the nanowires for the carrier transportation, the annealing process improved the contact between the nanowire interfaces. As a result, the contact resistance was reduced, and the potential barrier was lowered. Other important effects of the annealing process included an improvement of the nanowire crystallinity and a reduction in defects, which also significantly improved the photocurrent properties of the sensor.

Improvements of UV sensor performances from surface modifications have also been reported by other groups. For instance, Park et al. showed that a larger photocurrent value and faster photoresponse time were achieved for roughened ZnO nanorods in a UV photodetector (Park et al., 2011). They demonstrated that the surfaces of the nanorods could be roughened by immersing the nanorods in isopropyl alcohol (IPA) for 30 days. The etched areas of the nanorod surfaces from IPA contained defects state that enhanced the adsorption of oxygen molecules onto the surface. This condition resulted in a large quantity of oxygen molecules that adsorbed onto the nanorod surfaces.

Another method for increasing the sensor responsivity involved the surface passivation of ZnO nanorods by thin layer coating (e.g., with polyvinyl alcohol (PVA)). The idea is to increase the photoluminescence (PL) UV emission of the ZnO while reducing the green emission that is related to ZnO surface defects. Recent research on coating ZnO nanoparticles with PVA has shown a suppression in the number of defects evidenced by a reduction in the parasitic green emission (Qin et al., 2011). This characteristic increased the ratio of the photocurrent over the dark current compared to the uncoated ZnO particles. The coatings effectively decreased the number of holes in the deep level, which helped the UV-excited electrons to recombine with the holes in the valence band without being trapped in the deep-level defects of ZnO.

5.2 Role of nanorod array thickness

We investigated the performance of the UV sensor at different nanorod array thicknesses. In this study, we prepared the nanorod array films at different thicknesses by varying the immersion times from 1 to 5 h. In this case, we used a 100 ml solution in the vessel to grow the Al-doped ZnO nanorod arrays. We have previously shown that the volume of solution in the vessel affects the nanorod length or film thickness during the deposition process (Mamat et al., 2011). Therefore, it was expected that the film prepared for this study would be thinner than the nanorod array discussed in section 5.1. Figure 8 depicts FESEM images of the Al-doped ZnO nanorod arrays at different immersion times. The sizes of the nanorod diameters in the sample prepared after a 1 h immersion (Fig. 8(a)) ranged from 40 to 150 nm. Notably, the diameters of the nanorods remained almost unchanged after increasing the immersion time to 2, 4, and 5 h, as observed in Fig. 8(b), 8(c), and 8(d).

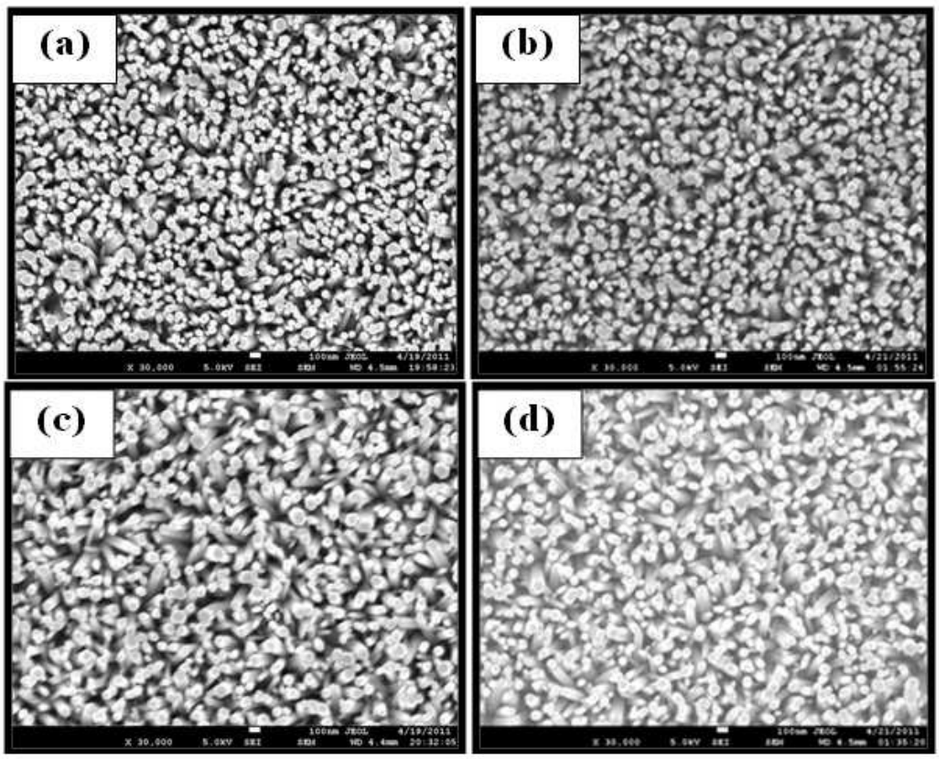

Fig. 8. Top-view FESEM images of Al-doped ZnO nanorod arrays prepared at immersion times of (a) 1, (b) 2, (c) 4, and (d) 5 h.

To investigate the growth behaviour, we performed thickness measurements to characterise the lengths of the nanorods, i.e., the film thicknesses that were grown with at different immersion times. The thicknesses of the nanorods were 629, 677, 727, 768, and 834 nm after being immersed for 1,2,3,4, and 5 hours, respectively. From this result, we concluded that the nanorod growth behaviour occurs primarily along the c-axis when the immersion process is carried out at longer times. It is interesting to note that the nanorod dimension increased only in length when immersed for longer times, without significantly affecting the size of the nanorod diameter. This result indicates that the controllable growth of the nanorods along the c-axis could be achieved under different immersion times using our sonicated sol-gel immersion method while maintaining the diameter sizes of the nanorods. It demonstrated that the sonication process provides a good dispersion process of the starting materials to produce a mixture of zinc-aluminium-hexamethylenetetramine (Zn-Al-HMT) complexes, which inhibit growth at the nonpolar surfaces of ZnO while promoting growth along the c-axis, or polar surface, at longer immersion times.

Figure 9 shows the photoresponse spectra of the Al-doped ZnO nanorod array-based UV sensor at different thicknesses. The photocurrent value of the UV sensor decreased with increasing film thickness up to 834 nm. The decrease in photocurrent value with film thickness also influenced the responsivity of the device, as it exhibited a lower value with thicker films. The responsivity of the device was calculated to be 2.13, 1.75, 1.21, 0.94, and 0.83 A/W for sensors with thicknesses of 629, 677, 727, 768, and 834 nm, respectively. Thicker films also increased the rise (decay) time constant of the devices. The rise (decay)

process time constants of the device were calculated to be 3(12), 4(13), 6(15), 8(16), and 9(20) s for 629, 677, 727, 768, and 834 nm-thick nanorod array-based UV sensors, respectively.

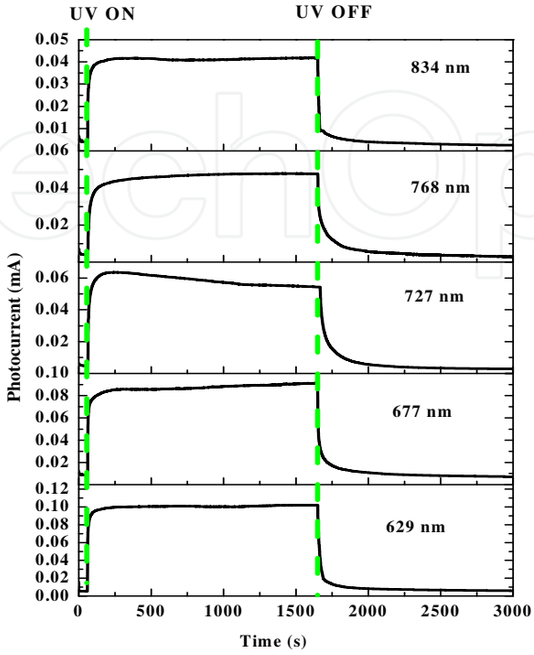

Fig. 9. UV photoresponse properties of Al-doped ZnO nanorod arrays at different thicknesses under a 365 nm, 750 μW/cm² UV light at 10 V bias voltage.

In the UV sensor, the film has an optimum thickness for effectively detecting UV irradiation. If the film is too thin, the UV light can pass through the film and not be fully absorbed because the transmittance depth of light is proportional to its wavelength. Therefore, the photocurrent value would be weak due to the low carrier photogeneration within the limited absorbed UV light. A thicker film should increase the UV absorption, which would result in an enhancement of the photocurrent value and responsivity of the UV sensor. However, an excessively thick film would saturate the UV absorption and would not contribute to an increase in photogenerated carriers. In this study, a reduction of responsivity of the sensor with increasing film thickness might be influenced by the extension of the diffusion lengths of the carriers to the metal contacts (Fu & Cao, 2006). An increase in film thickness should increase the recombination probability of the electron-hole pairs, leading to a decrease in photocurrent, and thus reducing the responsivity value of the UV sensor. This phenomenon might also contribute to a larger rise (decay) time constant of the device.

A similar observation of thickness-dependent UV photoconductive sensor was also reported by Shinde et al. when they produced a gallium (Ga)-doped ZnO thin-film-based UV photoconductive sensor fabricated using a spray pyrolysis method (Shinde & Rajpure, 2011, 2011). They found that by decreasing the Ga-doped ZnO thin film from 225 nm to 139 nm, the responsivity of the sensor at a 5 V bias voltage at 365 nm improved from 1125 A/W to 1187 A/W.

5.3 Aluminium doping effects

The doping process also plays an important role in the performance of the UV sensor. There are several elements that could be used as a dopant in the nanorods, such as gallium (Ga), indium (In), and aluminium (Al). In our study, we used Al ions doping because it could be easily incorporated into the ZnO lattice and because it enhanced some of the ZnO nanorod properties, such as optical transmittance and electrical conductivity. Furthermore, Al can serve as a donor and induce chemical defects, which tremendously improve the optical and electrical properties of ZnO (Yun & Lim, 2011).

Figure 10 shows the FESEM morphologies and cross-sectional images of undoped (Fig 10(a-c)) and Al-doped ZnO nanorod arrays (Fig. 10(d-e)). In this experiment, we sonicated 500 ml of the precursor solution in a smaller beaker to increase the ultrasonic power density applied to the solution. We observed that the diameter sizes of nanorods decreased after Al ions doping. The sizes of the undoped ZnO nanorods varied from 80 to 120 nm, while the sizes of the Al-doped ZnO nanorods ranged from 30 to 70 nm. The reduction in size may have originated from the different radii of Zn^{2+} and Al^{3+} ions, which are 0.074 nm and 0.054 nm, respectively. The existence of Al in the ZnO lattice may influence the attractive forces between the atoms and thus reduce the diameter sizes of the ZnO nanorod. A similar behaviour of the decrease in diameter was also reported by Hsu et al. (Hsu & Chen, 2010). We also observed that the diameter sizes of Al-doped ZnO nanorods were smaller than those of nanorods produced using a solution that was sonicated in a volume of 1000 ml, as discussed in section 5.1 and 5.2. We suspect that the mixing process between the precursor (i.e., zinc nitrate), stabiliser (i.e., HMT), and dopant (i.e., aluminium nitrate) was improved by the stronger and more intense ultrasonic irradiation.

Figure 11 shows the photoresponse spectra of undoped and Al-doped ZnO nanorod array-based UV photoconductive sensors under 365 nm UV illumination with an optical power density of 750 $\mu W/cm^2$. The spectra reveal that the Al-doped ZnO nanorod array-based UV sensor almost doubled the magnitude of the photocurrent compared to the undoped ZnO nanorod. The responsivity of the Al-doped ZnO-based UV sensor was 3.24 A/W, while the responsivity of the undoped ZnO-based UV sensor was 1.60 A/W. From the calculation results, we found that the rise (decay) process time constant of the undoped and Al-doped ZnO nanorod array-based UV sensors were 16(16) and 3(10) s, respectively. This result suggests that the Al-doped ZnO nanorod array improved the photoresponse of the sensor by increasing the responsivity and decreasing the rise (decay) process time constant.

By adding Al, the carrier concentration of ZnO nanostructures were improved because the substitution of Al^{3+} at the Zn^{2+} site created an extra free carrier in the process (Mridha & Basak, 2007, Fournier et al., 2008). Because of the high electron concentration, this condition reduced the barrier height between the Al-doped ZnO nanorod and the seed layer and between the film and the Al metal contact interface. This reduction initially allowed the photogenerated electrons to move more easily from the Al-doped ZnO nanorods to the seed layer, then from the seed layer back to the Al-doped ZnO nanorods underneath the metal contact, and finally to the metal contact. The flow of the photogenerated electrons during UV illumination is depicted in Fig. 12. Additionally, Al ions doping led to a suppression of defects in the film, such as zinc interstitials and oxygen vacancies, which served to increase the stability and performance of the Al-doped ZnO film-based sensor (Mamat et al., 2011, Sharma & Khare, 2010).

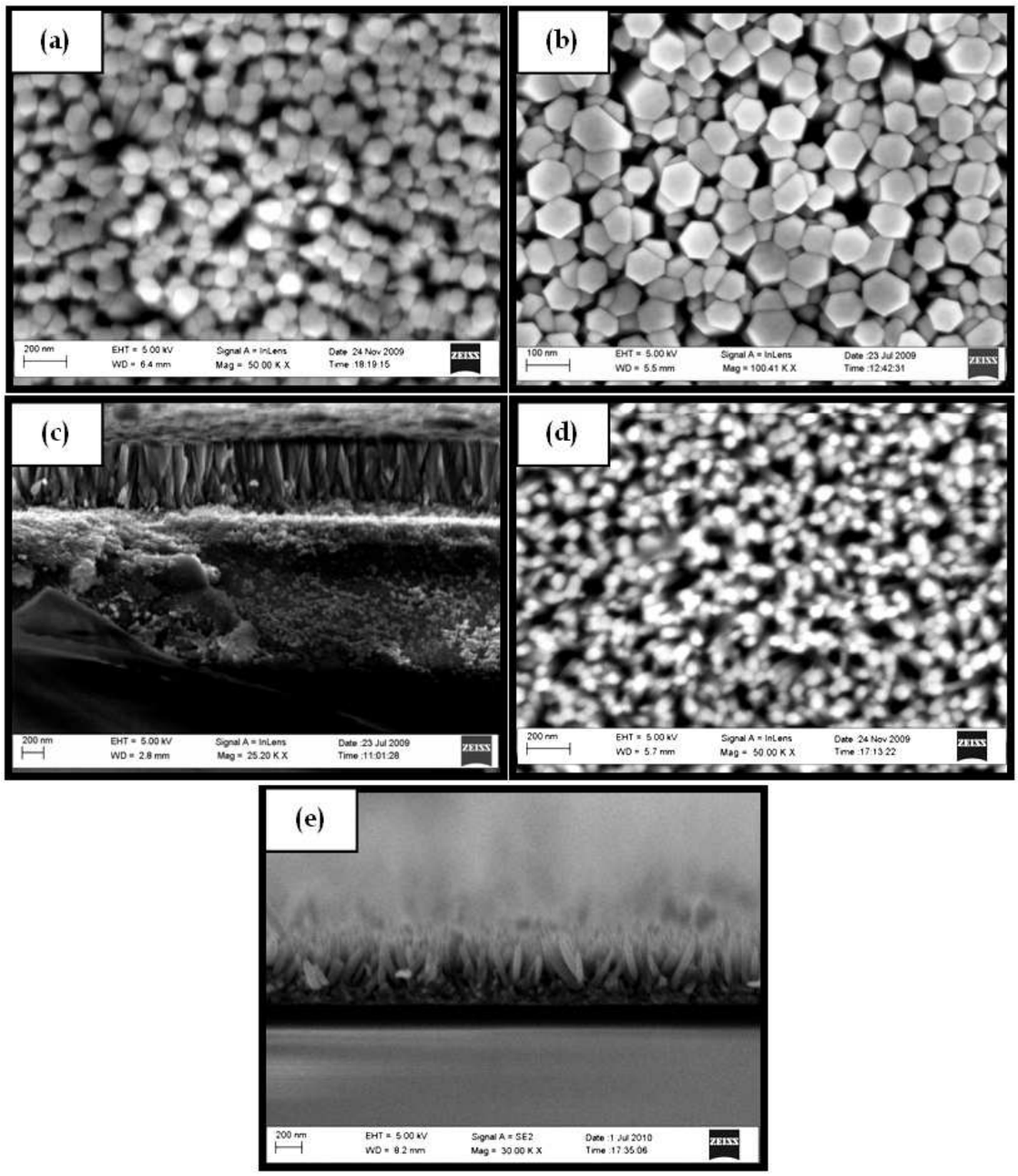

Fig. 10. FESEM images of undoped (a-c) and Al-doped ZnO (d-e) nanorod arrays prepared using 500 ml sonicated solution.

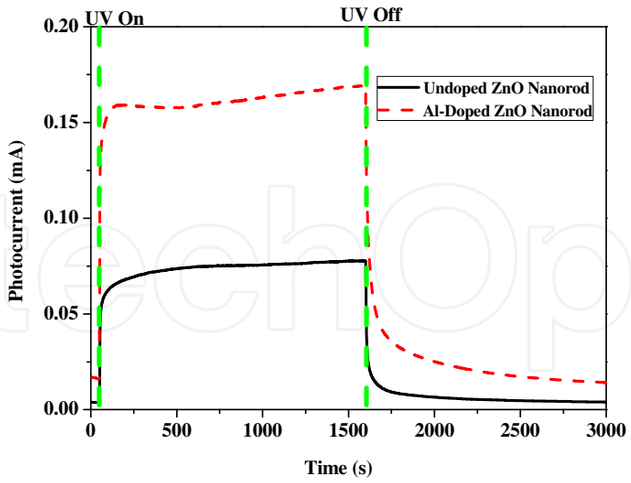

Fig. 11. The dependence of the photocurrent on operating time for undoped and Al-doped ZnO-nanorod-array-based UV photoconductive sensors under 365 nm UV light with a power density of 750 μW/cm² and a bias of 10 V.

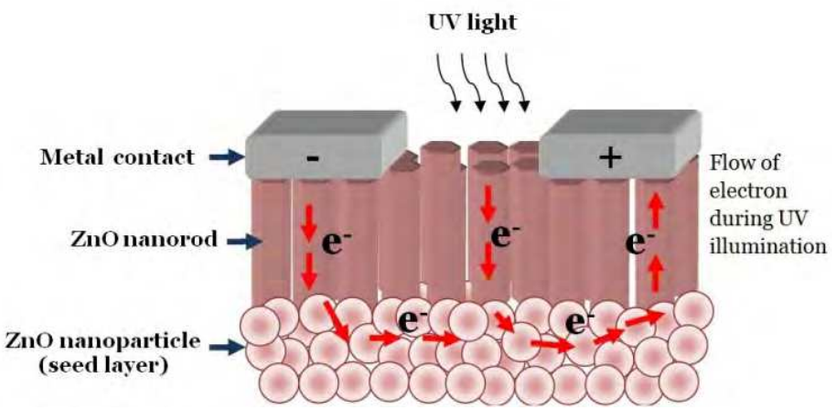

Fig. 12. Flow of photogenerated carrier during UV illumination in ZnO-nanorod-array-based UV photoconductive sensor

6. Conclusions

The performance of a UV photoconductive sensor using ZnO nanostructures, particularly ZnO nanorod arrays, was discussed. The problems related with grain boundaries and poor electron mobility have motivated researchers to develop ZnO nanostructure-based UV sensors. The ZnO nanostructures which could be prepared in many shapes such as nanorod and nanobelt might provide a way in improving electronic device performance through reducing grain boundaries concentration and increasing the electron mobility in the structure. Numerous techniques have been used to fabricate ZnO nanostructure-based UV sensors, such as radio frequency (RF) magnetron sputtering, chemical vapour deposition (CVD), sol-gel, molecular beam epitaxy (MBE), and pulsed laser deposition. Based on previous studies, the use of nanostructure materials for UV photoconductive sensor

applications have many advantages over bulk structures, including high gain, low power consumption, high sensitivity, reduced dimensionality, and the use of an extremely small fraction of the device's active materials. There are a number of factors that contribute to the high photosensitivity of nanostructure-based devices, such as the surface-to-volume ratio, surface defects, light trapping, and porosity. Current research has mainly focused on the fabrication of UV photoconductive sensors using smaller ZnO nanostructures that contribute to the large surface area of the sensing element and prolonging the carrier lifetime of the device during UV illumination to lower the charge-carrier recombination. The nanostructures that have high carrier mobility also have been used to improve the transit time of carriers, which results in the improvement of the device performance. A review of the current status of the UV photoconductive sensor found that ZnO nanorods are very promising nanostructures for UV detection due to their large surface area, high mobility, and good surface photochemistry. However, there are still many challenges in the fabrication of ZnO nanorod-based UV sensors because of certain ZnO defects that are produced during the fabrication process. These defects eventually contribute to a lower photoresponsivity, a low photogenerated carrier lifetime, and less effective UV light absorption properties of the ZnO-nanorod-array-based UV sensor. In this chapter, we have discussed the fabrication of ZnO-nanorod-array-based UV photoconductive sensors via ultrasonic-assisted sol-gel and immersion methods. The fabrication of ZnO nanorod arrays using a solution-based method is very attractive because of its simplicity, versatility, and low-temperature processing. We found that several factors influence the UV sensor performance, including surface treatment, film thickness, and doping of the ZnO nanorod arrays.

7. Acknowledgements

The authors would like to thank Universiti Teknologi MARA (UiTM) Malaysia, Ministry of Higher Education (MOHE) Malaysia, Jabatan Perkhidmatan Awam (JPA) Malaysia and Research Management Institute (RMI) of UiTM for financial support. The authors would also like to thank the Faculty of Applied Sciences (Mr. Hayub) and Faculty of Mechanical Engineering, UiTM for their FESEM and XRD facilities, respectively. The authors thank Mr. Shuhaimi Ahmad (UiTM technician), Mrs. Nurul Wahida (UiTM Asst. Science Officer) and Mr. Mohd Azlan Jaafar (UiTM technician) for their kind support during this research.

8. References

Lee, J.M.; et al. (2009). ZnO Nanorod−Graphene Hybrid Architectures for Multifunctional Conductors. *The Journal of Physical Chemistry C*, Vol.113, No.44, pp.19134, ISSN 1932-7447.

Galoppini, E.; et al. (2006). Fast Electron Transport in Metal Organic Vapor Deposition Grown Dye-sensitized ZnO Nanorod Solar Cells. *The Journal of Physical Chemistry B*, Vol.110, No.33, pp.16159, ISSN 1520-6106.

Park, W.; et al. (2011). Enhancement in the photodetection of ZnO nanowires by introducing surface-roughness-induced traps. *Nanotechnology*, Vol.22, No.20, pp.205204, ISSN 0957-4484.

Hullavarad, S.; et al. (2007). Ultra violet sensors based on nanostructured ZnO spheres in network of nanowires: a novel approach. *Nanoscale Research Letters*, Vol.2, No.3, pp.161, ISSN 1931-7573.

Soci, C.; et al. (2010). Nanowire Photodetectors. *Journal of Nanoscience and Nanotechnology*, Vol.10, No.3, pp.1430, ISSN 1533-4880.

Pimentel, A.; et al. (2006). Role of the thickness on the electrical and optical performances of undoped polycrystalline zinc oxide films used as UV detectors. *Journal of Non-Crystalline Solids*, Vol.352, No.9-20, pp.1448, ISSN 0022-3093.

Xu, Z.-Q.; et al. (2006). Ultraviolet photoconductive detector based on Al doped ZnO films prepared by sol-gel method. *Applied Surface Science*, Vol.253, No.2, pp.476, ISSN 0169-4332.

Zheng, X.G.; et al. (2006). Photoconductive ultraviolet detectors based on ZnO films. *Applied Surface Science*, Vol.253, No.4, pp.2264, ISSN 0169-4332.

Jun, J.H.; et al. (2009). Ultraviolet photodetectors based on ZnO nanoparticles. *Ceramics International*, Vol.35, No.7, pp.2797, ISSN 0272-8842.

Liu, J.M.; et al. (2007). Effect of grain size on the electrical properties of ultraviolet photodetector with ZnO/diamond film structure. *Journal of Crystal Growth*, Vol.300, No.2, pp.353, ISSN 0022-0248.

Yang, W.; et al. (2003). Compositionally-tuned epitaxial cubic $Mg_xZn_{1-x}O$ on Si(100) for deep ultraviolet photodetectors *Applied Physics Letters*, Vol.82, pp.3424, ISSN 1077-3118

Yuan, B.; et al. (2011). High photosensitivity and low dark current of photoconductive semiconductor switch based on ZnO single nanobelt. *Solid-State Electronics*, Vol.55, No.1, pp.49, ISSN 0038-1101.

Jiang, D.; et al. (2011). Ultraviolet photodetectors with MgZnO nanowall networks grown by molecular beam epitaxy on Si(1 1 1) substrates. *Materials Science and Engineering: B*, Vol.176, No.9, pp.736, ISSN 0921-5107.

Soci, C.; et al. (2007). ZnO Nanowire UV Photodetectors with High Internal Gain. *Nano Letters*, Vol.7, No.4, pp.1003, ISSN 1530-6984.

Mamat, M.H.; et al. (2011). Fabrication of ultraviolet photoconductive sensor using a novel aluminium-doped zinc oxide nanorod-nanoflake network thin film prepared via ultrasonic-assisted sol-gel and immersion methods. *Sensors and Actuators A: Physical*, Vol.In Press, Corrected Proof, ISSN 0924-4247.

Su, Y.K.; et al. (2009). Ultraviolet ZnO Nanorod Photosensors. *Langmuir*, Vol.26, No.1, pp.603, ISSN 0743-7463.

Zheng, X.G.; et al. Photoconductive properties of ZnO thin films grown by pulsed laser deposition. *Journal of Luminescence*, Vol.122-123, pp.198, ISSN 0022-2313.

Lupan, O.; et al. (2010). Ultraviolet photoconductive sensor based on single ZnO nanowire. *physica status solidi (a)*, Vol.207, No.7, pp.1735, ISSN 1862-6319.

Chai, G.Y.; et al. (2011). Fabrication and characterization of an individual ZnO microwire-based UV photodetector. *Solid State Sciences*, Vol.13, No.5, pp.1205, ISSN 1293-2558.

Niarchos, G.; et al. (2010). Growth of ZnO nanorods on patterned templates for efficient, large-area energy scavengers. *Microsystem Technologies*, Vol.16, No.5, pp.669, ISSN 0946-7076.

Suslick, K.S.; et al. (1991). Sonochemical synthesis of amorphous iron. *Nature*, Vol.353, No.6343, pp.414, ISSN 0028-0836.

Mishra, P.; et al. (2010). Growth mechanism and photoluminescence property of flower-like ZnO nanostructures synthesized by starch-assisted sonochemical method. *Ultrasonics Sonochemistry*, Vol.17, No.3, pp.560, ISSN 1350-4177.

Jia, X.; et al. (2010). Using sonochemistry for the fabrication of hollow ZnO microspheres. *Ultrasonics Sonochemistry*, Vol.17, No.2, pp.284, ISSN 1350-4177.

Mazloumi, M.; et al. (2009). Ultrasonic induced photoluminescence decay in sonochemically obtained cauliflower-like ZnO nanostructures with surface 1D nanoarrays. *Ultrasonics Sonochemistry*, Vol.16, No.1, pp.11, ISSN 1350-4177.

Mamat, M.H.; et al. (2010). Novel synthesis of aligned Zinc oxide nanorods on a glass substrate by sonicated sol-gel immersion. *Materials Letters*, Vol.64, No.10, pp.1211, ISSN 0167-577X.

Mamat, M.H.; et al. (2010). Influence of doping concentrations on the aluminum doped zinc oxide thin films properties for ultraviolet photoconductive sensor applications. *Optical Materials*, Vol.32, No.6, pp.696, ISSN 0925-3467.

Lee, S.; et al. (2007). Fabrication of a solution-processed thin-film transistor using zinc oxide nanoparticles and zinc acetate. *Superlattices and Microstructures*, Vol.42, No.1-6, pp.361, ISSN 0749-6036.

Shinde, S.S. & Rajpure, K.Y. (2011). High-performance UV detector based on Ga-doped zinc oxide thin films. *Applied Surface Science*, Vol.257, No.22, pp.9595, ISSN 0169-4332.

Qiu, M.; et al. (2009). Growth and properties of ZnO nanorod and nanonails by thermal evaporation. *Applied Surface Science*, Vol.255, No.7, pp.3972, ISSN 0169-4332.

Mamat, M.H.; et al. (2011). Controllable Growth of Vertically Aligned Aluminum-Doped Zinc Oxide Nanorod Arrays by Sonicated Sol-Gel Immersion Method depending on Precursor Solution Volumes. *Japanese Journal of Applied Physics*, Vol.50, No.6, pp.06GH04, ISSN 1347-4065.

Khusaimi, Z.; et al. (2010). Controlled Growth of Zinc Oxide Nanorods by Aqueous-Solution Method. *Synthesis and Reactivity in Inorganic, Metal-Organic, and Nano-Metal Chemistry*, Vol.40, No.3, pp.190 ISSN 1553-3174.

Guo, M.; et al. (2005). Hydrothermal growth of well-aligned ZnO nanorod arrays: Dependence of morphology and alignment ordering upon preparing conditions. *Journal of Solid State Chemistry*, Vol.178, No.6, pp.1864, ISSN 0022-4596.

Chen, Y.W.; et al. (2009). Size-Controlled Synthesis and Optical Properties of Small-Sized ZnO Nanorods. *The Journal of Physical Chemistry C*, Vol.113, No.18, pp.7497, ISSN 1932-7447.

Giri, P.K.; et al. (2010). Effect of ZnO seed layer on the catalytic growth of vertically aligned ZnO nanorod arrays. *Materials Chemistry and Physics*, Vol.122, No.1, pp.18, ISSN 0254-0584.

Lupan, O.; et al. (2007). Nanofabrication and characterization of ZnO nanorod arrays and branched microrods by aqueous solution route and rapid thermal processing. *Materials Science and Engineering: B*, Vol.145, No.1-3, pp.57, ISSN 0921-5107.

Sugunan, A.; et al. (2006). Zinc oxide nanowires in chemical bath on seeded substrates: Role of hexamine. *Journal of Sol-Gel Science and Technology*, Vol.39, No.1, pp.49, ISSN 0928-0707.

Laudise, R.A. & Ballman, A.A. (1960). Hydrothermal synthesis of zinc oxide and zinc sulfide. *The Journal of Physical Chemistry*, Vol.64, No.5, pp.688, ISSN 0022-3654.

Laudise, R.A.; et al. (1965). Impurity content of synthetic quartz and its effect upon mechanical Q. *Journal of Physics and Chemistry of Solids*, Vol.26, No.8, pp.1305, ISSN 0022-3697.

De la Rosa, E.; et al. (2007). Controlling the Growth and Luminescence Properties of Well-Faceted ZnO Nanorods. *The Journal of Physical Chemistry C*, Vol.111, No.24, pp.8489, ISSN 1932-7447.

Lee, J.; et al. (2010). Improvement of optical properties of post-annealed ZnO nanorods. *Physica E: Low-dimensional Systems and Nanostructures*, Vol.42, No.8, pp.2143, ISSN 1386-9477.

Lin, B.; et al. (2001). Green luminescent center in undoped zinc oxide films deposited on silicon substrates. *Applied Physics Letters*, Vol.79, No.7, pp.943, ISSN 1077-3118

Li, Y.; et al. (2009). Fabrication of ZnO nanorod array-based photodetector with high sensitivity to ultraviolet. *Physica B: Condensed Matter*, Vol.404, No.21, pp.4282, ISSN 0921-4526.

Kim, K.-P.; et al. (2011). Thermal annealing effects on the dynamic photoresponse properties of Al-doped ZnO nanowires network. *Current Applied Physics*, Vol.11, No.6, pp.1311, ISSN 1567-1739.

Qin, L.; et al. (2011). Enhanced ultraviolet sensitivity of zinc oxide nanoparticle photoconductors by surface passivation. *Optical Materials*, Vol.33, No.3, pp.359, ISSN 0925-3467.

Fu, Y. & Cao, W. (2006). Preparation of transparent TiO_2 nanocrystalline film for UV sensor. *Chinese Science Bulletin*, Vol.51, No.14, pp.1657, ISSN 1001-6538.

Shinde, S.S. & Rajpure, K.Y. (2011). Fast response ultraviolet Ga-doped ZnO based photoconductive detector. *Materials Research Bulletin*, Vol.46, No.10, pp.1734, ISSN 0025-5408.

Yun, S. & Lim, S. (2011). Effect of Al-doping on the structure and optical properties of electrospun zinc oxide nanofiber films. *Journal of Colloid and Interface Science*, Vol.360, No.2, pp.430, ISSN 0021-9797.

Hsu, C.-H. & Chen, D.-H. (2010). Synthesis and conductivity enhancement of Al-doped ZnO nanorod array thin films. *Nanotechnology*, Vol.21, No.28, pp.285603, ISSN 0957-4484.

Mridha, S. & Basak, D. (2007). Aluminium doped ZnO films: electrical, optical and photoresponse studies. *Journal of Physics D: Applied Physics*, Vol.40, No.22, pp.6902, ISSN 0022-3727.

Fournier, C.; et al. (2008). Effects of substrate temperature on the optical and electrical properties of Al:ZnO films. *Semiconductor Science and Technology*, Vol.23, No.8, pp.085019, ISSN 0268-1242.

Sharma, B.K. & Khare, N. (2010). Stress-dependent band gap shift and quenching of defects in Al-doped ZnO films. *Journal of Physics D: Applied Physics*, Vol.43, No.46, pp.465402, ISSN 0022-3727.

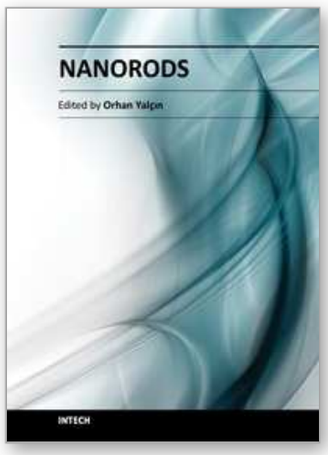

Nanorods

Edited by Dr. Orhan Yalçın

ISBN 978-953-51-0209-0

Hard cover, 250 pages

Publisher InTech

Published online 09, March, 2012

Published in print edition March, 2012

The book "Nanorods" is an overview of the fundamentals and applications of nanosciences and nanotechnologies. The methods described in this book are very powerful and have practical applications in the subjects of nanorods. The potential applications of nanorods are very attractive for bio-sensor, magneto-electronic, plasmonic state, nano-transistor, data storage media, etc. This book is of interest to both fundamental research such as the one conducted in Physics, Chemistry, Biology, Material Science, Medicine etc., and also to practicing scientists, students, researchers in applied material sciences and engineers.

How to reference

In order to correctly reference this scholarly work, feel free to copy and paste the following:

Mohamad Hafiz Mamat, Zuraida Khusaimi, Musa Mohamed Zahidi and Mohamad Rusop Mahmood (2012). ZnO Nanorod Arrays Synthesised Using Ultrasonic-Assisted Sol-Gel and Immersion Methods for Ultraviolet Photoconductive Sensor Applications, Nanorods, Dr. Orhan Yalçın (Ed.), ISBN: 978-953-51-0209-0, InTech, Available from: http://www.intechopen.com/books/nanorods/zno-nanorod-arrays-synthesised-using-ultrasonic-assisted-sol-gel-and-immersion-methods-for-ultraviol

INTECH
open science | open minds

InTech Europe
University Campus STeP Ri
Slavka Krautzeka 83/A
51000 Rijeka, Croatia
Phone: +385 (51) 770 447
Fax: +385 (51) 686 166
www.intechopen.com

InTech China
Unit 405, Office Block, Hotel Equatorial Shanghai
No.65, Yan An Road (West), Shanghai, 200040, China
中国上海市延安西路65号上海国际贵都大饭店办公楼405单元
Phone: +86-21-62489820
Fax: +86-21-62489821

IntechOpen